Versão do arquivo anexado / Version of attached file:

Versão do Editor / Published Version

Mais informações no site da editora / Further information on publisher's website:

https://www.physiology.org/doi/full/10.1152/ajpheart.00379.2018

DOI: 10.1152/ajpheart.00379.2018

Direitos autorais / Publisher's copyright statement:

RESEARCH ARTICLE | *Vascular Biology and Microcirculation*

Peri/epicellular protein disulfide isomerase-A1 acts as an upstream organizer of cytoskeletal mechanoadaptation in vascular smooth muscle cells

Leonardo Y. Tanaka,[1] Thaís L. S. Araujo,[1] Andres I. Rodriguez,[1,2] Mariana S. Ferraz,[3]
Vitor B. Pelegati,[4] Mauro C. C. Morais,[5] Aline M. dos Santos,[6] Carlos L. Cesar,[4] Alexandre F. Ramos,[5]
Adriano M. Alencar,[3] and Francisco R. M. Laurindo[1]

[1]*Vascular Biology Laboratory, Heart Institute, University of São Paulo School of Medicine, São Paulo, Brazil;* [2]*Group of Research and Innovation in Vascular Health, Department of Basic Sciences, Faculty of Sciences, University of Bío-Bío, Chillán, Chile;* [3]*Institute of Physics, University of São Paulo, São Paulo, Brazil;* [4]*"Gleb Wataghin" Institute of Physics, University of Campinas, Campinas, Brazil;* [5]*Escola de Artes, Ciências e Humanidades e Núcleo de Estudos Interdisciplinares em Sistemas Complexos, Departamento de Radiologia e Oncologia e Centro de Pesquisa Translacional em Oncologia - Instituto do Cancer do Estado São Paulo, Faculdade de Medicina, Universidade de São Paulo, São Paulo, Brazil; and* [6]*Department of Structural and Functional Biology, Institute of Biology, University of Campinas, Campinas, Brazil*

Submitted 21 June 2018; accepted in final form 7 November 2018

Tanaka LY, Araujo TL, Rodriguez AI, Ferraz MS, Pelegati VB, Morais MC, Santos AM, Cesar CL, Ramos AF, Alencar AM, Laurindo FR. Peri/epicellular protein disulfide isomerase-A1 acts as an upstream organizer of cytoskeletal mechanoadaptation in vascular smooth muscle cells. *Am J Physiol Heart Circ Physiol* 316: H566–H579, 2019. First published November 30, 2018; doi:10.1152/ajpheart.00379.2018.—Although redox processes closely interplay with mechanoresponses to control vascular remodeling, redox pathways coupling mechanostimulation to cellular cytoskeletal organization remain unclear. The peri/epicellular pool of protein disulfide isomerase-A1 (pecPDIA1) supports postinjury vessel remodeling. Using distinct models, we investigated whether pecPDIA1 could work as a redox-dependent organizer of cytoskeletal mechanoresponses. In vascular smooth muscle cells (VSMCs), pecPDIA1 immunoneutralization impaired stress fiber assembly in response to equibiaxial stretch and, under uniaxial stretch, significantly perturbed cell repositioning perpendicularly to stretch orientation. During cyclic stretch, pecPDIA1 supported thiol oxidation of the known mechanosensor β_1-integrin and promoted polarized compartmentalization of sulfenylated proteins. Using traction force microscopy, we showed that pecPDIA1 organizes intracellular force distribution. The net contractile moment ratio of platelet-derived growth factor-exposed to basal VSMCs decreased from 0.90 ± 0.09 (IgG-exposed controls) to 0.70 ± 0.08 after pecPDI neutralization ($P < 0.05$), together with an enhanced coefficient of variation for distribution of force modules, suggesting increased noise. Moreover, in a single cell model, pecPDIA1 neutralization impaired migration persistence without affecting total distance or velocity, whereas siRNA-mediated total PDIA1 silencing disabled all such variables of VSMC migration. Neither expression nor total activity of the master mechanotransmitter/regulator RhoA was affected by pecPDIA1 neutralization. However, cyclic stretch-induced focal distribution of membrane-bound RhoA was disrupted by pecPDI inhibition, which promoted a nonpolarized pattern of RhoA/caveolin-3 cluster colocalization. Accordingly, FRET biosensors showed that pecPDIA1 supports localized RhoA activity at cell protrusions versus perinuclear regions. Thus, pecPDI acts as a thiol redox-dependent organizer and noise reducer mechanism of cytoskeletal repositioning, oxidant generation, and localized RhoA activation during a variety of VSMC mechanoresponses.

NEW & NOTEWORTHY Effects of a peri/epicellular pool of protein disulfide isomerase-A1 (pecPDIA1) during mechanoregulation in vascular smooth muscle cells (VSMCs) were highlighted using approaches such as equibiaxial and uniaxial stretch, random single cell migration, and traction force microscopy. pecPDIA1 regulates organization of the cytoskeleton and minimizes the noise of cell alignment, migration directionality, and persistence. pecPDIA1 mechanisms involve redox control of β_1-integrin and localized RhoA activation. pecPDIA1 acts as a novel organizer of mechanoadaptation responses in VSMCs.

cytoskeleton; mechanobiology; protein disulfide isomerase; redox; vascular smooth muscle cells

INTRODUCTION

Vascular remodeling is an essential determinant of lumen caliber in physiological adaptations and disease conditions (7). However, the processes that orchestrate this vascular response are still poorly understood. Our group has worked with the proposal that redox signaling exerts such a coordinating role (36). Since remodeling is closely dependent on cellular mechanoresponses (17), which are themselves strongly redox regulated, we (36) recently proposed a mechanobiological/redox paradigm of vascular remodeling. Intrinsic to this model is the notion that redox-dependent events modulate mechanosensing, transmission, and effector responses with a sufficient degree of temporospatial coherence to render the overall phenomenon predictably responsive to redox-related interventions. However, understanding the redox mechanisms coupling such mechanosignaling to cellular cytoskeletal organization remains a significant gap in such model.

We (35) recently showed that the peri/epicellular pool of protein disulfide isomerase-A1 (pecPDIA1) supports expansive arterial remodeling during vascular repair after injury. PDIA1 is the prototype of the PDI family of thioredoxin superfamily redox chaperones responsible for disulfide introduction into nascent proteins at the endoplasmic reticulum, the canonical location of most PDIs (2, 15, 34). The pecPDIA1

pool, estimated to be <2% of the total cellular PDIA1 pool, is externalized mainly through Golgi-independent subcellular routes in vascular cells (1, 6) and mediates thiol redox events related to thrombosis, virus internalization, and cell adhesion, among others (2, 15, 34). Intracellular PDIA1 is essentially required for agonist-driven activation of Nox NADPH oxidases (18). Emerging evidence (2, 15, 34) suggests that PDIA1 functionally converges with cytoskeletal regulation during Nox1 NADPH oxidase-dependent vascular smooth muscle cell (VSMC) migration (29). In this signaling capacity, PDIA1 and possibly other PDIs are unlikely, from the kinetic standpoint, to act as mass peroxide sensors (26) and have instead been proposed as redox signaling adaptors (22). Our results in the remodeling model indicate that PDIA1 supports intracellular oxidant generation. At the same time, pecPDIA1 displays a thiol reductase effect on cell surface integrins (36), which is similar to the well-reported thiol redox effects of pecPDIA1 on platelet or endothelial cell integrins during thrombus formation (15). Meanwhile, during short-term shear stress in endothelial cells, we showed an opposite effect, that is, α_5-integrin oxidation (1). Overall, such effects promote organization of the vascular cell cytoskeleton and extracellular matrix architecture, optimizing vascular stiffness.

These effects raised the hypothesis that pecPDIA1 could act as a more general redox organizer of cytoskeletal mechanoresponses. This was supported by initial evidence indicating that pecPDIA1 neutralization disrupts actin cytoskeleton reorganization upon cyclic stretch in VSMCs or shear stress in endothelial cells (35). In the present study, we explored this hypothesis in VSMCs under distinct models of mechanoadaptive regulation and investigated possible pathways associated with pecPDIA1-mediated mechanisms.

METHODS

Ethical approval. This study was approved by the Scientific Research and Ethics Committees of the Heart Institute and School of Medicine, University of São Paulo, Brazil, no. SDC 3334/08/085 and CEUA (Animal Experiments Committee, Protocol 1086/09).

Cell culture and protocol for cyclic stretch. Primary VSMCs isolated from the rabbit thoracic aorta or rat aortic VSMC lineage (A7R5) were used. For equibiaxial stretch experiments, rabbit VSMCs from *passages 3–8* were cultured on collagen type I flexible membranes (Flexcell) and stretched (10–12%, 1 Hz/24 h) or kept static with anti-PDI or nonimmune mouse IgG (1 μg/ml). Uniaxial stretch (8–10%, 1 Hz) was performed in Flexcell chambers. The stretch pattern is similar to an analogous study from the literature and mimics physiological ranges in large-conductance vessels (10). Migration and part of the uniaxial stretch experiments were performed in A7R5 cells. For all other experiments, primary cells were used.

Actin fiber analysis. Detailed analysis of F-actin fiber thickness was performed in VSMCs using Hessian matrix-based analysis. Briefly, six transversal lines per cell were selected for analysis using ImageJ's "line tool." Pixel intensity through such lines is plotted using the "Plot Profile" tool. Fluorescent labeled actin fibers are represented as curvilinear structures depicting local intensity variations (minima or maxima). The intensity profile is analyzed using a Hessian matrix, which describes the second-order information or curvature of these intensity variations and allows one to extract line-like information from the input data. Using the ImageJ plugin FeatureJ, the following parameters were acquired: "largest eigenvalue of Hessian tensor" option and "absolute eigenvalue comparison" option; the "smoothing scale" factor is set to 0.5. These parameters generate a resulting image of largest eigenvalues compared with the absolute values of the Hessian matrixes. Determination of separated fiber thickness is ob-

tained following nearest neighbor deconvolution. Intensity matrixes are processed through a slope peak detection formula. A fiber intensity histogram is plotted based on fiber/peak intensities measured in each line scan normalized to maximum values obtained in a selected image. This measurement was adapted from Sathyanesan et al. (32), who reported nerve fiber quantification. Here, for actin fiber quantification, the histogram bin size was adapted to 2 arbitrary units of normalized fluorescence intensity.

Cortical actin thickness was calculated by measuring the integrated density fluorescence corrected to cell area and fluorescent background, as previously reported (3).

Cell orientation. The orientation of A7R5 VSMCs maintained at static or uniaxial stretch conditions, as described above, was measured at 4 and 24 h using the plugin Orientation J (ImageJ). Individual cells were traced, and the cell positions relative to their major axis were analyzed. Fully aligned cells represented perpendicularly oriented cells relative to stretch direction. Aligned cells were assumed as 0°, and intermediate cell position ranged from −90° to 90°. Statistical comparisons were performed in cells that were fully (0°) and near fully (−10 and 10°) aligned. An average of ~100 cells was measured in two fields from three independent experiments.

Extracellular PDI and β_1-integrin free thiol measurement. VSMCs were incubated in serum-free medium, and extracellular free thiols were labeled with 200 μmol/l 3-(N-maleimidopropionyl)biocytin (MPB) for 1 h at 4°C. Unreacted MPB was quenched with 400 μmol/l glutathione and 800 μmol/l iodoacetamide, respectively. For oxidized extracellular thiol detection, cells were incubated with membrane-impermeable p-chloromercurphenylsulfonate (pCMPS; 0.5 mM for 10 min at 37°C), and disulfides then were reduced with membrane-impermeable Tris(2-carboxyethyl)phosphine hydrochloride (TCEP; 2 mM for 10 min at 37°C). Finally, labeling of the freshly reduced thiols was conducted with MPB as described above (Fig. 2D, schema). For both redox measurements, cells were lysed in the presence of protease inhibitors, sonicated, and incubated with streptavidin magnetic beads (2 mg/ml) overnight at 4°C. Beads were washed followed by specific protein detection by Western blot analysis.

Traction force microscopy. VSMCs (A7R5, 750 cells) were plated in a polyacrylamide-based soft substrate (4.7 kPa) containing fluorescent beads on its surface and coated with collagen type I (200 μg/ml) and kept in a culture chamber at 37°C coupled to a Leica DMI4000D fluorescence microscope (Wetzlar, Germany). Such parameters were based on physiological stiffness ranges (8) and studies using vascular cells (9, 20). After 12 h, cells were starved and incubated with neutralizing PDI antibody or control nonimmune IgG (1 μg/ml). Traction forces were calculated from displacement fields provoked by cells on the fluorescent substrate markers, as previously published, through MatLab software (4). For the displacement field, we compared two fluorescent images of the substrate with and without cells. Single cell images were acquired using phase contrast at basal condition and fluorescent detection at baseline, after incubation with platelet-derived growth factor (PDGF; 25 ng/ml, 5 min), and after cell removal with trypsin. Traction force intensity and distributions were calculated based on bead displacement through the MatLab software. Images were acquired using ×20 objective.

Force vector length determination. We were interested in the force underlying cell movement, which we denoted as a force vector, that is, the vector from the cell's centroid to the cell's center of traction. The centroid of the cell was defined as the average of the coordinates x and y of the pixels within its membrane. The ith pixel in a cell's image has coordinates denoted by (x_i, y_i). The coordinates of the centroid are

$$(x_C, y_C) = N^{-1} \sum_{i=1}^{N} (x_i, y_i),$$ where N is the total number of pixels within

the limits of the cell's image[1]. To determine the cell's center of traction, we computed the "center of mass" of the intensities of the cell's traction field. We denoted the traction intensity at the position of the ith pixel of the cell image as T_i. Thus, the coordinates of the

center of traction are $(x_T, y_T) = T^{-1} \sum_{i=1}^{N} T_i(x_i, y_i)$, where $T = \sum_{i=1}^{N} T_i$ is the sum of the traction at all pixels within the cell's image[2].

The force vector of the jth image of a cell has coordinates $F_j = (x_T - x_C, y_T - y_C)_j$, with subscript j labeling the cell's image from 1 to M. The force vector magnitude can be obtained as usual: $|F_j| = \sqrt{(x_T - x_C)_j^2 + (y_T - y_C)_j^2}$, and its angle to the horizontal axis is $\theta_j = \operatorname{atan}\dfrac{(y_T - y_C)_j}{(x_T - x_C)_j}$. With this algorithm, one can compute the average and standard deviation on $|F_j|$ and θ_j for M cell images.

Immunofluorescence. Primary VSMCs (1×10^5) from the rabbit aorta or A7R5 VSMCs were cultivated in six-well plates coated with collagen type I (Flexcell), fixed with paraformaldehyde (4% for 10–20 min at room temperature), permeabilized or not with 0.1% Triton X-100 (10 min at room temperature), blocked with BSA (4% for 1 h at room temperature), and incubated overnight with primary antibodies followed by fluorescein-conjugated secondary antibodies, phalloidin and DAPI for F-actin and nuclei staining, respectively. Glass slides were placed over the flexible membrane in PBS-glycerol [1:1 (vol/vol)] and analyzed in a confocal laser microscope (LSM510 Zeiss Axio Vision). For protein sulfenylation detection, cells were incubated with 5 mM dimedone at the last hour of static or stretch period. Negative controls without dimedone and without anti-dimedone were performed.

Measurement of oxidant generation. Dihydroethidium (DHE)-derived oxidation product measurement was performed using a HPLC coupled system as previously described (14) with minor modifica-
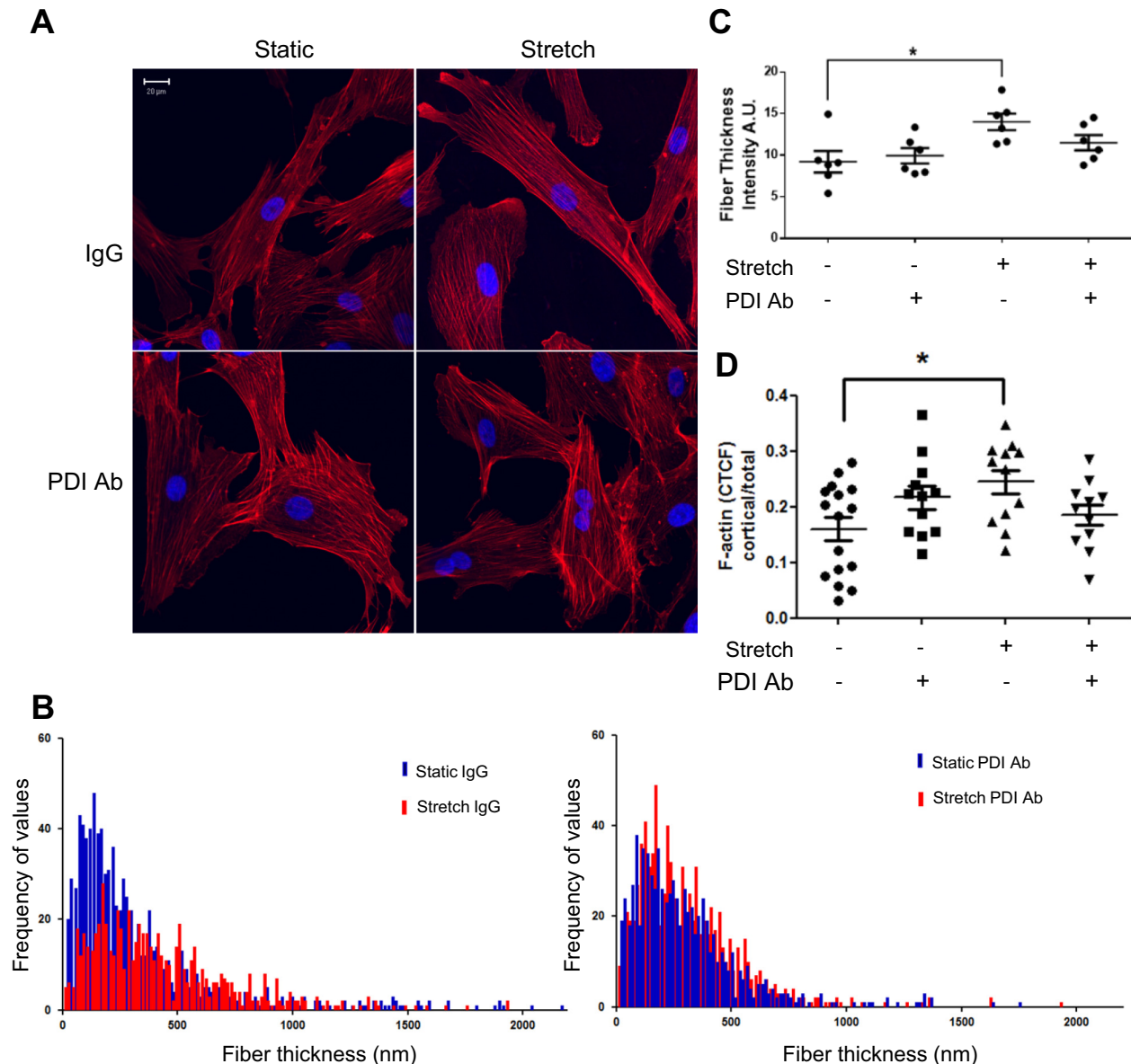

Fig. 1. Peri/epicellular pool of protein disulfide isomerase-A1 (pecPDIA1) supports mechanoresponse-associated cytoskeletal organization in cyclic stretch-exposed vascular smooth muscle cells (VSMCs). *A*: primary rabbit aortic VSMCs under static conditions or submitted to 24-h biaxial cyclic stretch (10–12%, 1 Hz) were incubated with IgG or PDI antibody (PDI Ab; both 1 µg/ml, starting 1 h before stretch), and F-actin filaments (Alexa-phalloidin 635 nm, red) were analyzed in paraformaldehyde-fixed cells. Nuclei are shown in blue (DAPI). *B* and *C*: actin fiber thickness was measured through Hessian matrix-based analysis (see METHODS). *B*: fiber thickness frequency distribution showing static (blue bars) versus stretch (red bars) conditions of control IgG (*left*) and PDI Ab-treated cells (*right*). *C*: graph depicting values of whole fiber measurements of ≥2 cells from 3 independent experiments. AU, arbitrary units. *D*: graph depicting cortical to total F-actin fluorescence [corrected total cell fluorescence (CTCF)]. *P < 0.05 vs. static IgG.

tions. To measure oxidant production during stretch, cells were washed twice with HBSS, and 50 µM DHE was added during the last 10 min of treatment (static or stretch). Peaks of 2-hydroxiethidium and ethidium were corrected for consumed DHE.

Random single cell migration. VSMCs were grown in 12-well plates at low confluence (1.25×10^3 cells/cm^2) and analyzed using an inverted Zeiss Axiovert 200 microscope (×10 magnification at 37°C and 5% CO_2). Time lapse recording started 1 h after stimulation with vehicle or PDGF (25 ng/ml). Four to five fields per well were imaged and followed at 10-min intervals over 16 h with a cooled charge-coupled device video camera operated by Axiovision image-analysis software. Migration parameters calculated from each individual cell, including total migration distance, distance to origin, rate of migration, and directional persistence of cell migration, were determined from time lapse movies for at least 25 independent cells. Total migration distance represents the sum of distances between each measurement over a period of 16 h. Distance to origin was determined as the net translocation between the initial position and the final position observed during a 16-h period. Directional persistence was calculated as the ratio between distance to origin and total migration distance during a 16-h period. At least 5 cells/field were measured, and the results are expressed as the mean of each parameter calculated from the individual cells (~25 cells).

Immunoblot analysis. Proteins (30 to 50 µg aliquots) were separated by SDS-PAGE in 12% polyacrylamide gels and transferred to a nitrocellulose membrane. The membrane was incubated with 5% nonfat milk for 2 h and overnight at 4°C with primary antibodies followed by fluorescein-conjugated secondary antibodies for 1 h at room temperature. The antibody-protein complex was quantified through infrared fluorescent detector (Li-Cor-Odyssey) or using chemiluminescence for biotin-horseradish peroxidase detection of total MPB labeling. For assessment of sulfenylated susbtrates, dimedone incubation was performed as described above. Lysis buffer was supplemented with 200 U/ml catalase, 100 µM diethylene triamine pentaacetic acid, and 5 mM iodoacetamide. Dimedone protein adducts were detected under nonreducing conditions.

Total RhoA activity. RhoA absorbance was assayed with a G-LISA kit (Cytoskeleton) according to the manufacturer's protocol.

Distribution of RhoA activation. Local RhoA activation was measured using the plasmid biosensor (RhoA-FLARE, Addgen) coding full-length RhoA at the COOH terminus connected to yellow fluorescent protein (YFP) followed by a flexible sequence attached to cyan fluorescent protein (CYP) and a Rho-binding domain portion from Rhotekin at the NH$_2$ terminus (28). Briefly, when RhoA assumes its GTP-bound active form, the Rho-binding domain binds to RhoA, forcing the approximation of YFP and CFP, which induces fluorescence resonance energy transfer (FRET; see schema in Fig. 5D). FRET intensity was quantified by fluorescence lifetime microscopy (FLIM) of the donor CFP. Lifetime fluorescence at perinuclear re-

gions and cell protrusions was measured using Becker and Hickl software. Positive and negative controls were performed by transfecting cells, respectively, with plasmids coding for YFP linked to CFP through a 15-amino acid-long linker or for the individual separated fluorescent proteins, as previously described (27). Images were acquired with a Zeiss LSM780-NLO microscope (Carl Zeiss, Wetzlar, Germany). VSMCs were transfected with 1 µg of RhoA-FLARE and 500 ng for positive and negative controls, both using lipofectamine. Analyses were performed after 24-h transfection followed by 12-h starvation in paraformaldehyde-fixed cells (4%, 20 min).

Statistical analysis. Data are presented as means ± SE. Comparisons between groups presenting normal distribution were performed by an unpaired Student's t-test in the case of two groups (such as for net contractile moment and alignment with CN01). In the remaining cases, in which three or more groups were involved, data were analyzed using one-way ANOVA with a Newman-Keuls post hoc test using GraphPad Prism 6.0 (GraphPad Software, San Diego, CA). The force vector length ratio, which presented non-normal distribution, was analyzed through a Mann-Whitney test. The significance level for all comparisons was 5%.
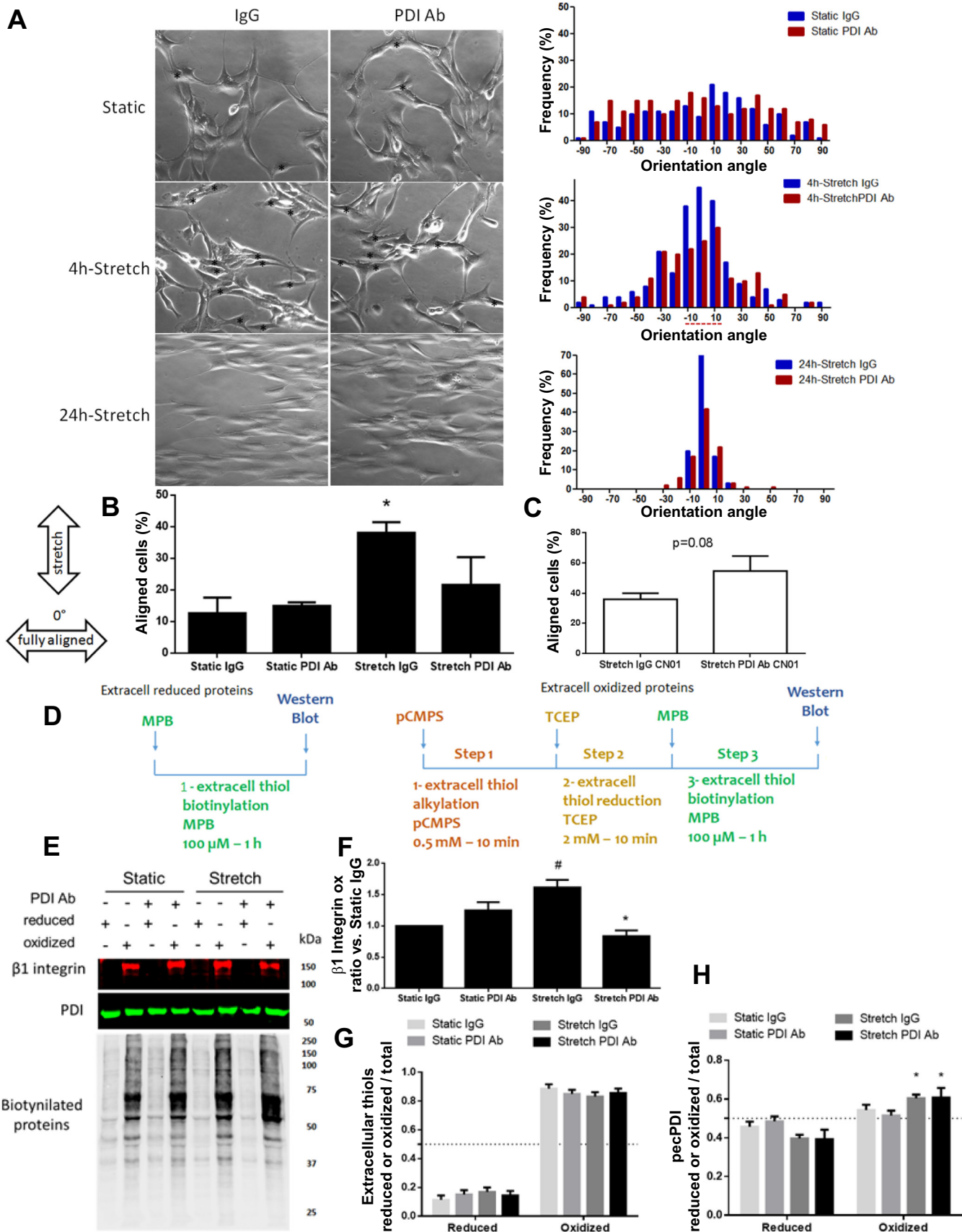
RESULTS

pecPDIA1 regulates VSMC responses to stretch. In a previous study (35), we showed that pecPDIA1 is required for an organized cytoskeletal response in both VSMCs and endothelial cells subjected to biaxial stretch and shear stress, respectively. Here, we initially extended these results in primary VSMCs from the rabbit aorta subjected to biaxial stretch by performing a detailed analysis of F-actin assembly (Fig. 1A). Our results show that mechanical stretch decreased the population of thinner fibers, indicating stretch-induced fiber thickening (Fig. 1B, *left*), whereas pecPDI inhibition prevented such an effect (Fig. 1B, *right*). Total and cortical fiber thickness measurement showed that only stretch IgG was increased compared with the control static condition (Fig. 1, C and D). The number of fibers was unaffected by either stretch or PDI antibody (data not shown). This indicates that the actin cytoskeleton fiber rearrangement was impaired by pecPDI.

Overall, these results indicate that pecPDIA1 is involved in proximal mechanisms of mechanoresponse organization after direct force stimulation in VSMCs.

pecPDIA1 minimizes noise in VSMC repositioning to uniaxial stretch. To further investigate whether pecPDIA1 regulates localized responses to stretch in distinct models, we submitted VSMCs to uniaxial stretch, which is known to promote cell realignment orthogonally to stretch (Fig. 2A, *bottom* arrows).

Fig. 2. Peri/epicellular pool of protein disulfide isomerase-A1 (pecPDIA1) supports vascular smooth muscle cell (VSMC) reorientation to uniaxial stretch by mechanisms involving β$_1$-integrin oxidation. A: VSMCs (A7R5) were submitted to uniaxial stretch for 4 or 24 h or maintained under static conditions in the presence of control IgG or PDI antibody (PDI Ab; 1 µg/ml, both 1-h preincubation). Stretch direction and cell orientation after chronic stretch treatment are shown by arrows at the *bottom left*. Cell positioning was measured using Orientation J/ImageJ software, which assumes fully aligned cells as 0°. Black asterisks at static or 4-h stretch images highlight cells at near full/full alignment. Histograms of static and stretched (for 4 or 24 h) cells showing cell orientation distribution are shown at the *top right*. B: graph showing cell orientation at near (-10 or $10°$) or full ($0°$) aligned angles comparing static versus 4-h stretch. *$P < 0.05$ vs. other groups ($n > 100$ cells from 3 independent experiments). C: graph showing cell alignment demonstrating the effect of RhoA activator treatment (CN01; 0.5 U/ml) added during 4-h stretch. D–H: reduced and oxidized pools of extracellular proteins were analyzed in 4-h uniaxial stretched/static cells with or without pecPDIA1 inhibition (as described in A). D: a brief protocol schema. Further details are described in METHODS: the reduced pool was measured by 3-(N-maleimidopropionyl)biocytin (MPB) incubation immediately after stimulus and oxidized pool derivatized first by thiol alkylation with nonpermeable p-chloromercurphenylsulfonate (pCMPS) followed by reduction with Tris(2-carboxyethyl)phosphine hydrochloride (TCEP) and then labeling of the newly reduced thiols with MPB. Biotin was pulled down with streptavidin conjugated with magnetic beads and detected with specific antibodies to β$_1$-integrin, PDI (RL90), or biotin-horseradish peroxidase. Cells were washed three times with PBS before MPB or pCMPS incubation. E: Western blot analysis of β$_1$-integrin, PDI, or extracellular protein thiol labeling. F: graph of oxidized β$_1$-integrin. #$P < 0.05$ for stretch IgG vs. all other conditions; *$P < 0.05$ for stretch PDI Ab vs. static conditions. G: graph showing reduced or oxidized total thiols. H: graph of reduced or oxidized pecPDI. *$P < 0.05$ for stretch IgG and stretch PDI Ab vs. its respective reduced group. $n = 3$–4 independent experiments.

Our results showed that pecPDIA1 neutralization perturbed cell repositioning to stretch, leading to a significant impairment of collective realignment at a distinct time course (Fig. 2*A*, please see cell images and histograms at *right*), presenting marked effects at 4 h of stretch treatment (Fig. 2*B*). Importantly, such an effect was prevented by forced RhoA activation with CN01 (Fig. 2*C*). The amount of stretch-induced cell alignment was unassociated with cell loss (data not shown). To explore potential targets of pecPDIA1 during uniaxial stretch, we addressed pecPDIA1-dependent changes in the redox state of cell surface β_1-integrin, since integrins are known to be closely involved with mechanoresponses, including directional migration and cell repositioning (31). In addition, pecPDIA1 has been shown to redox regulate integrin activation in different cell types (15). Using a modified assay for extracellular

thiol redox state (Fig. 2*D*), we showed that β_1-integrin thiols are oxidized by VSMC cyclic stretch. Meanwhile, pecPDIA1 inhibition significantly prevented such oxidation (Fig. 2, *E* and *F*), suggesting that pecPDIA1 supports a thiol oxidase effect during uniaxial stretch response. Stretch increased pecPDI oxidation, with no further detectable effect of PDI antibody incubation (Fig. 2*H*). Stretch-induced extracellular thiol oxidation was not a global phenomenon, as shown by their total detection with MPB labeling in resting and stretched samples (Fig. 2*G*). These results are in line with a similar documented effect of short-term shear stress in endothelial cells (1).

pecPDIA1 organizes the pattern of oxidant-rich subcompartments. Detection of thiol oxidase effects of pecPDIA1 during stretch, as well as during short-term shear stress in endothelial cells (35), is not obvious, given the well-known pecPDIA1 reduc-
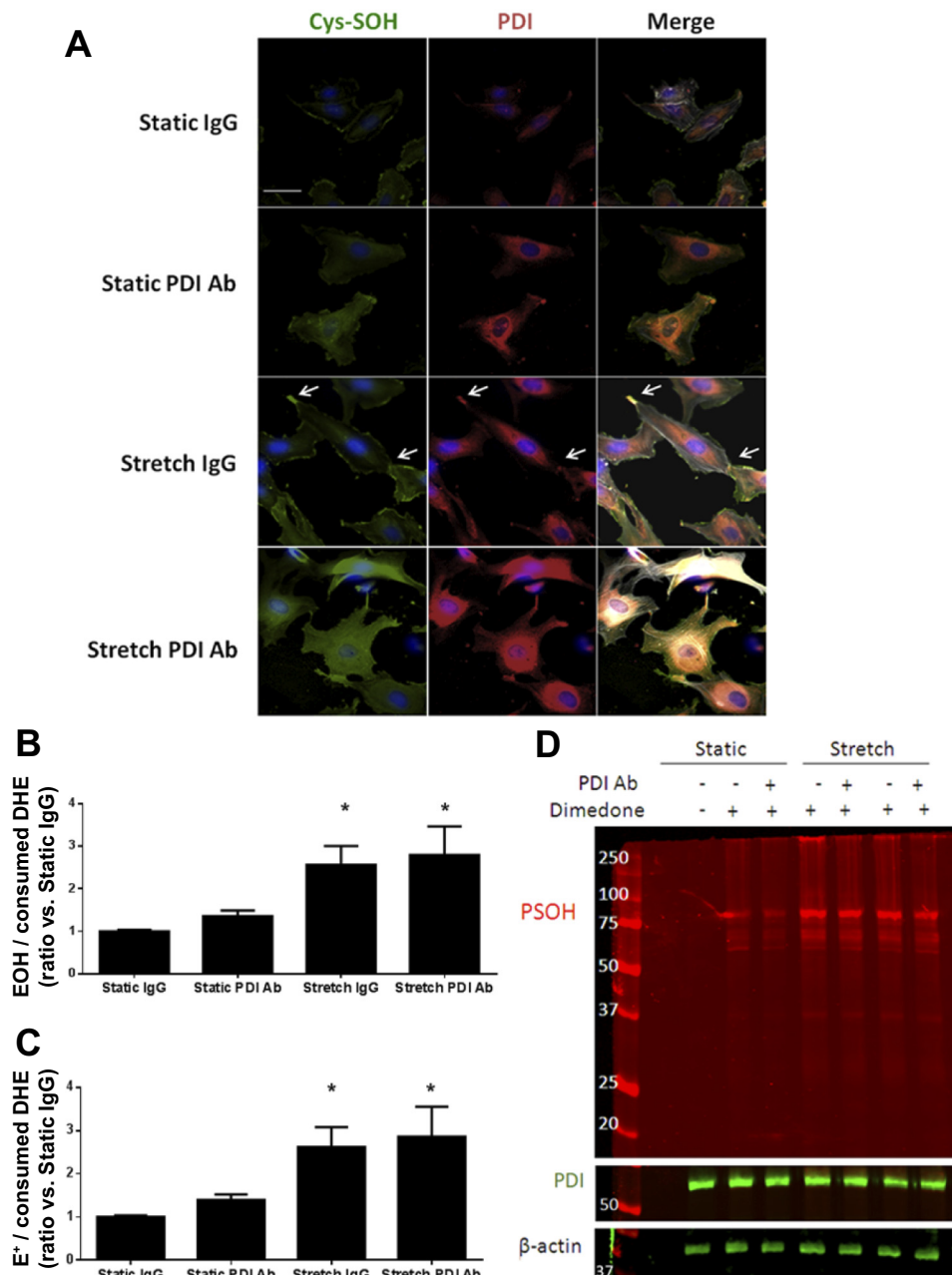

Fig. 3. Uniaxial stretch promotes compartmentalized distribution of protein disulfide isomerase-A1 (PDIA1) and sulfenate-rich proteins. Detection of protein sulfenic acid adducts (P-SOH or Cys-SOH) and PDI was performed in static and 4-h stretched cells (as in Fig. 2). One hour before the end of the stimulus, dimedone (5 mM) was added to the cells and P-SOH was labeled with anti-dimedone, as shown in green (*left*). PDI was labeled in red using a non-neutralizing antibody against the COOH terminus (*middle*). Merged images with nuclei (blue, DAPI) and F-actin (white, phalloidin) are shown on the *right*. White arrows highlight the peripheral distribution of PDI in P-SOH-rich areas induced by uniaxial stretch. Representative images are from 3 independent experiments. Negative controls without dimedone incubation were performed in all experiments and were used to set up the anti-dimedone labeling. *B* and *C*: static and 4-h stretched vascular smooth muscle cells (VSMCs) were incubated with dihydroethidium (DHE; 50 μM) at the last 10 min of treatment, and 2-hydroxyethidium (EOH; *B*) and ethidium (E$^+$; *C*) formation were measured. *P < 0.05 vs. the static group. $n = 3$ independent experiments. *D*: VSMCs were treated as described in *A*, and protein expression of dimedone-protein adducts (red) and PDI (green) was performed under nonreducing conditions. β-Actin was used as a loading control. Representative images are from 3 independent experiments.

tase effects previously reported in several circumstances (21), including our own data during vessel remodeling (35). Since mechanostimuli associate with oxidant generation (36) and PDIA1 is closely involved in agonist-stimulated Nox activation (13), we hypothesized that during cyclic stretch pecPDIA1 could associate with oxidant-rich cell subcompartments. Protein sulfenic acid formation can be regarded as a specific index of oxidant-induced thiol redox modification, which was indeed used to probe local oxidant generation in mechanorelated cell migration (5) and adhesion (12). We showed that uniaxial stretch promoted enrichment of the protein sulfenic acid pool

in localized cell subcompartments, which colocalized with PDIA1 in regions of apparent actin remodeling (Fig. 3A). This pattern was disrupted by pecPDIA1 inhibition, which promoted a diffuse relocation of sulfenylated proteins, even to some extent under static conditions, suggesting that pecPDIA1 organizes the distribution of oxidant-rich compartments at the cell periphery in association with mechanoresponses. In parallel, pecPDIA1 appears to be targeted to such prooxidant environments during cytoskeletal remodeling associated with normal cell repositioning to uniaxial stretch. Such an effect on local rather than global oxidant protein distribution was rein-
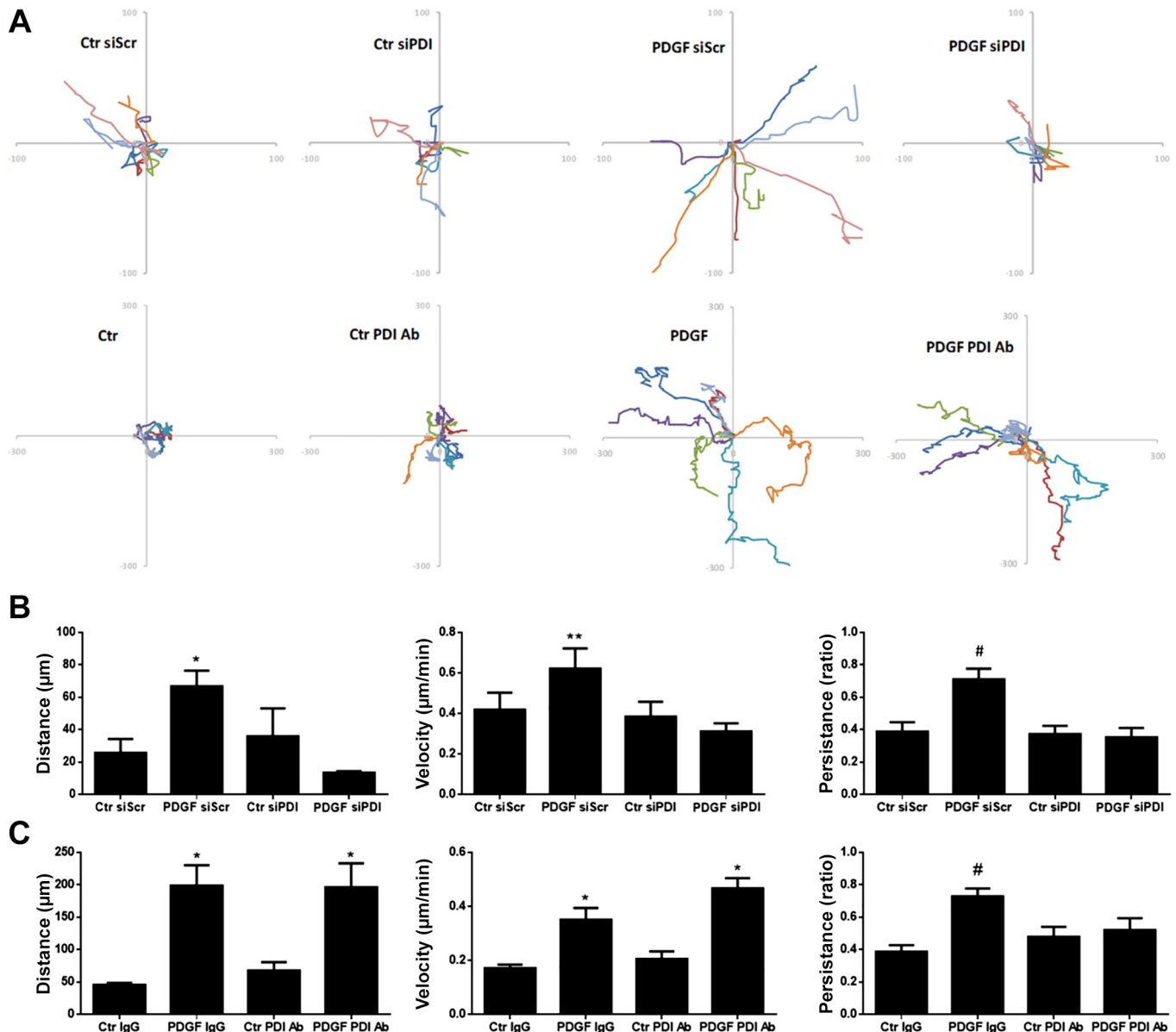

Fig. 4. Peri/epicellular pool of protein disulfide isomerase-A1 (pecPDIA1) effects on directional platelet-derived growth factor (PDGF)-driven vascular smooth muscle cell (VSMC) migration. A: random single cell migration of A7R5 VSMCs measured at baseline and during PDGF incubation (25 ng/ml) under physiological conditions (37°C, 5% CO_2 for 16 h). Data are shown after PDI silencing with siRNA [siPDI vs. scrambled control sequence (Scr), top] or in the presence of PDI antibody (PDI Ab; 1 μg/ml or nonimmune control IgG, bottom) during the migration protocol. Each colored line represents independent cell trajectories (7 cells/condition) plotted from the center position of the nuclei, with measurements every 10 min. The ordinate and abscissa indicate distances (in μm). B: graphs showing total distance (left), mean velocity (middle), and migration persistence (right) in control or PDI-silenced cells. Migration persistence was calculated by the mean ratio between distance to origin (D_{origin}) to total distance (D_{total}). *$P < 0.05$ vs. control siScr and PDGF siPDI; **$P < 0.05$ vs. PDGF siPDI; #$P < 0.05$ vs. control groups and PDGF siPDI. C: same graph set as shown in B for IgG or PDI Ab incubation. *$P < 0.05$ vs. control groups; #$P < 0.05$ vs. control and PDGF PDI Ab groups. Data are means ± SE of ≥7 cells from 3 independent experiments.
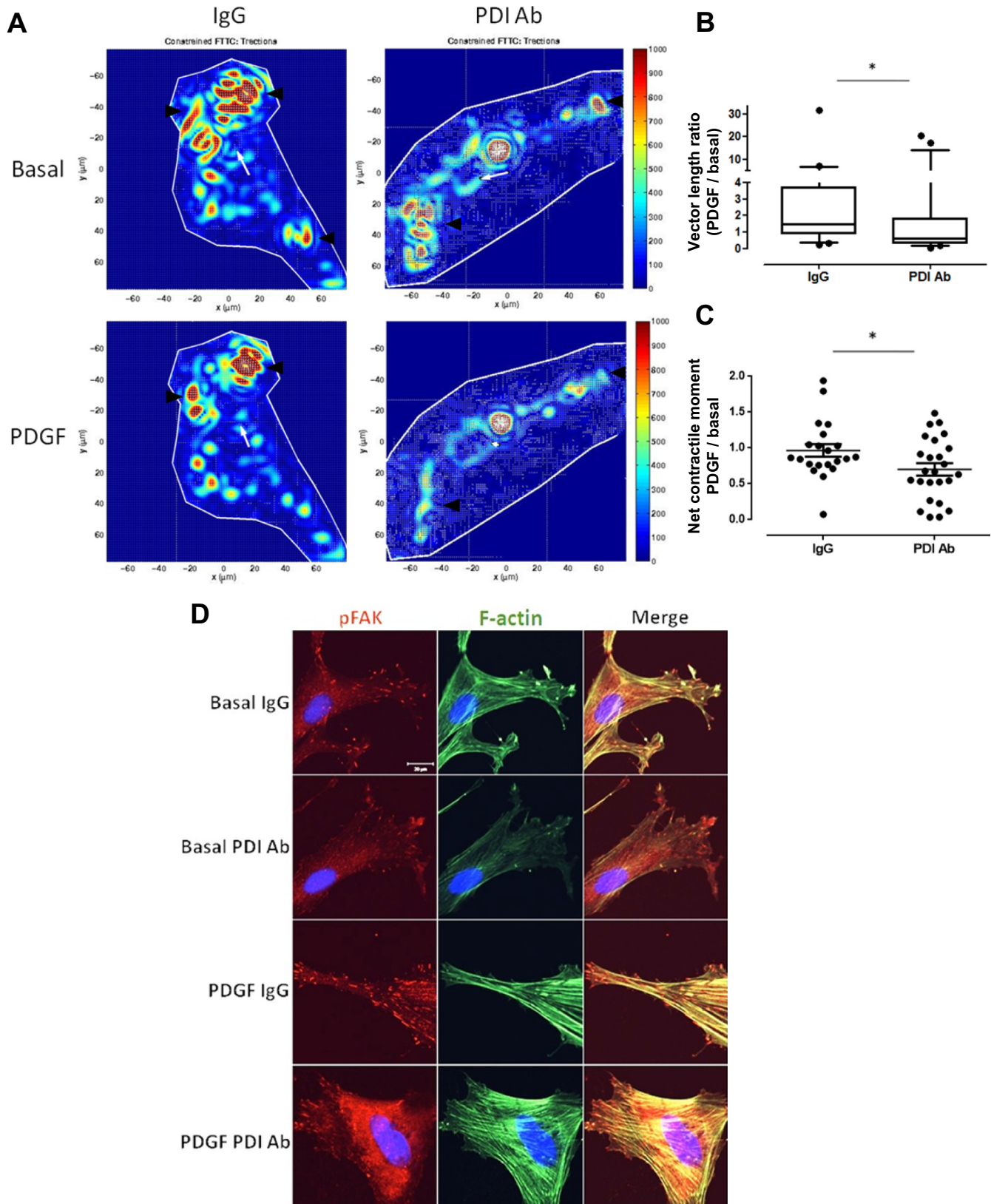
forced by the negligible effect of pecPDI on stretch-stimulated total oxidant generation (Fig. 3, *B* and *C*) and sulfenylated protein-dimedone adduct determination (Fig. 3*D*). Of note, despite the apparent increase in PDI and sulfenylated protein fluorescence upon cell stretch and/or exposure to PDI antibody (Fig. 3*A*), Western blot analysis indicated that total PDI levels were unchanged (Fig. 3*D*). A similar discrepancy between PDI fluorescence and Western blot analysis was previously documented by us (29).

pecPDIA1 acts as noise suppressor in polarity organization during VSMC migration. Having shown the effects of pecPDIA1 on mechanoadaptive responses, we investigated the occurrence and possible mechanisms of pecPDIA1-mediated cytoskeletal dynamics in a more complex physiologically relevant model such as cell migration. We (29) previously showed that total PDI silencing by siRNA markedly prevented agonist-stimulated VSMC migration in wound healing and transwell assays. Here, we addressed pecPDIA1 effects in a model of random single VSMC migration, which allows inferences regarding dynamic migration persistence and cell polarization (Fig. 4*A*). In line with our reported results (29), PDIA1 loss of function with siRNA markedly disrupted PDGF-induced VSMC migration, with decreases in total distance, migration velocity, and migration persistence (Fig. 4*B*). In contrast, pecPDIA1 neutralization did not affect migration velocity or total distance (Fig. 4*C*, *left* and *middle* graphs, respectively). However, the persistence of migration, which relates to a coordinated organization of dynamic cytoskeletal remodeling, was significantly decreased (Fig. 4*C*, *right*), suggesting that pecPDIA1 supports specific aspects of cytoskeletal organization responsible for persistence maintenance, in a way reminiscent of the decreased noise in cellular repositioning from the experiments shown in Fig. 2*A*.

During cell migration and spreading, noise in the distribution of traction and expansion forces is minimized by a concerted organization of cycles of cytoskeleton and focal adhesion assembly and disassembly (9). Using traction force microscopy, we investigated the distribution of intracellular forces at baseline and during incubation with PDGF. VSMCs seeded in a collagen matrix at physiological viscosity (4.7 kPa) organized a polarized pattern of force distribution (Fig. 5*A*), which was partially disrupted upon short-term (5-min) incubation with PDGF, consistent in both cases with the known organized cytoskeleton/focal adhesion assembly and disassembly cycles discussed above. Importantly, both at baseline and after PDGF incubation, pecPDIA1 inhibition markedly disrupted such polarized pattern of force generation, which was reflected in enhanced changes of the force vector length (see METHODS) as well as lower total force production after PDGF by pecPDIA1 inhibition (Fig. 5, *B* and *C*, respectively). In addi-

tion, enhanced noise of force redistribution occurred after pecPDIA1 inhibition, as reflected by the higher coefficient of variation of the resultant force vector length after PDGF (235.1% after pecPDI inhibition vs. 105.8% in controls; Fig. 5*B*). Overall, these results indicate that pecPDIA1 is closely involved in the coordinated organization of cytoskeletal changes that allow noise minimization during cellular movement. Since these changes also involve focal adhesions, we assessed the pattern of phospho-FAK (pFAK; Tyr[397]) fluorescence (Fig. 5*D*). The well-structured adhesion sites staining for pFAK at baseline and after PDGF were significantly disrupted after PDI antibody incubation: their number was markedly reduced, and they underwent cluster formation at the cell periphery at baseline while showing diffuse cytosolic staining after PDGF.

pecPDIA1 regulates site-specific RhoA activation. Our results so far implicate pecPDIA1 in the regulation of the polarized pattern of cytoskeletal organization in a variety of models exploring distinct aspects of these processes. We next investigated potential mechanisms associated with pecPDIA1 effects. We focused on the key mechanotransducer RhoA, which is known to act downstream of integrins and closely connected with several effects targeted by pecPDIA1 inhibition, such as response to external forces, cytoskeleton assembly, migration, and force production. Our results showed that neither total expression nor total RhoA activity was affected by PDI antibody incubation in stretched VSMCs versus their respective IgG controls (Fig. 6, *A* and *B*). Given the localized nature of pecPDIA1 effects noted so far, we hypothesized that local rather than global RhoA signaling could be disturbed. Early RhoA activation during stretch has been reported to occur at distinct membrane domains, initially in caveolae and at later stages outside of caveolae (19). Therefore, we addressed whether pecPDIA1 affects the spatial convergence of RhoA and caveolae in fixed but nonpermeabilized cells submitted or not to 24-h cyclic stretch. RhoA/caveolin-3 clusters displayed differential topology upon stretch, being preferentially located at the perinuclear region, whereas at the cell periphery/membranes, there was evidence for RhoA dissociation from caveolae (white arrows in the stretch IgG condition in Fig. 6*C*; see cell images plus graph at the *bottom*). Importantly, pecPDI neutralization disrupted such a pattern of RhoA membrane location (reminiscent of its activation) observed upon stretch, with persistence of RhoA/caveolin-3 clustering scattered at all cell locations. In addition, upon PDI antibody exposure in static conditions, there was an increase in global clustering of RhoA and caveolin-3 without a localization pattern (Fig. 6*C*).

Since membrane location is a hallmark of Rho-GTPase activation, these results suggest that pecPDIA1 may regulate

---

Fig. 5. Peri/epicellular pool of protein disulfide isomerase-A1 (pecPDIA1) supports distribution of cell forces and focal adhesions. *A*: measurement of traction force distribution of A7R5 vascular smooth muscle cells (VSMCs) with or without pecPDIA1 inhibition (1-h preincubation at 1 µg/ml). First, cells were plated in an acrylamide gel (4.7-kPa stiffness) containing fluorescent beads and functionalized with collagen type I (200 µg/ml). Real-time traction force production was then measured at baseline and after short-term (5-min) platelet-derived growth factor (PDGF) exposure (25 ng/ml). After removal of cells with trypsin, traction forces were calculated by bead displacement measurements using MatLab. The scale color heatmap (in kPa) shows the force and intensity of force distribution under all described conditions. Black arrowheads highlight the force redistribution after PDGF treatment. *B* and *C*: force vector length (*B*) and net contractile moment (*C*) after PDGF treatment corrected by the basal condition. *P < 0.05 vs. IgG ratio of PDGF vs. the basal condition. *n* = 20–21 cells. Vector length is shown by the white arrow at traction force (*A*). *D*: VSMCs cultivated under the same conditions as described for traction force microscopy measurements (except for fluorescent bead inclusion) were stained for phosphorylated (p)FAK (Tyr[397], *left*, Alexa 546 nm, red), F-actin (phallodin 635 nm, *middle*, green), and nuclei staining with DAPI (blue). Merged channels are shown on the *right*. Scale bar = 20 µm. Representative images from 3 independent experiments.
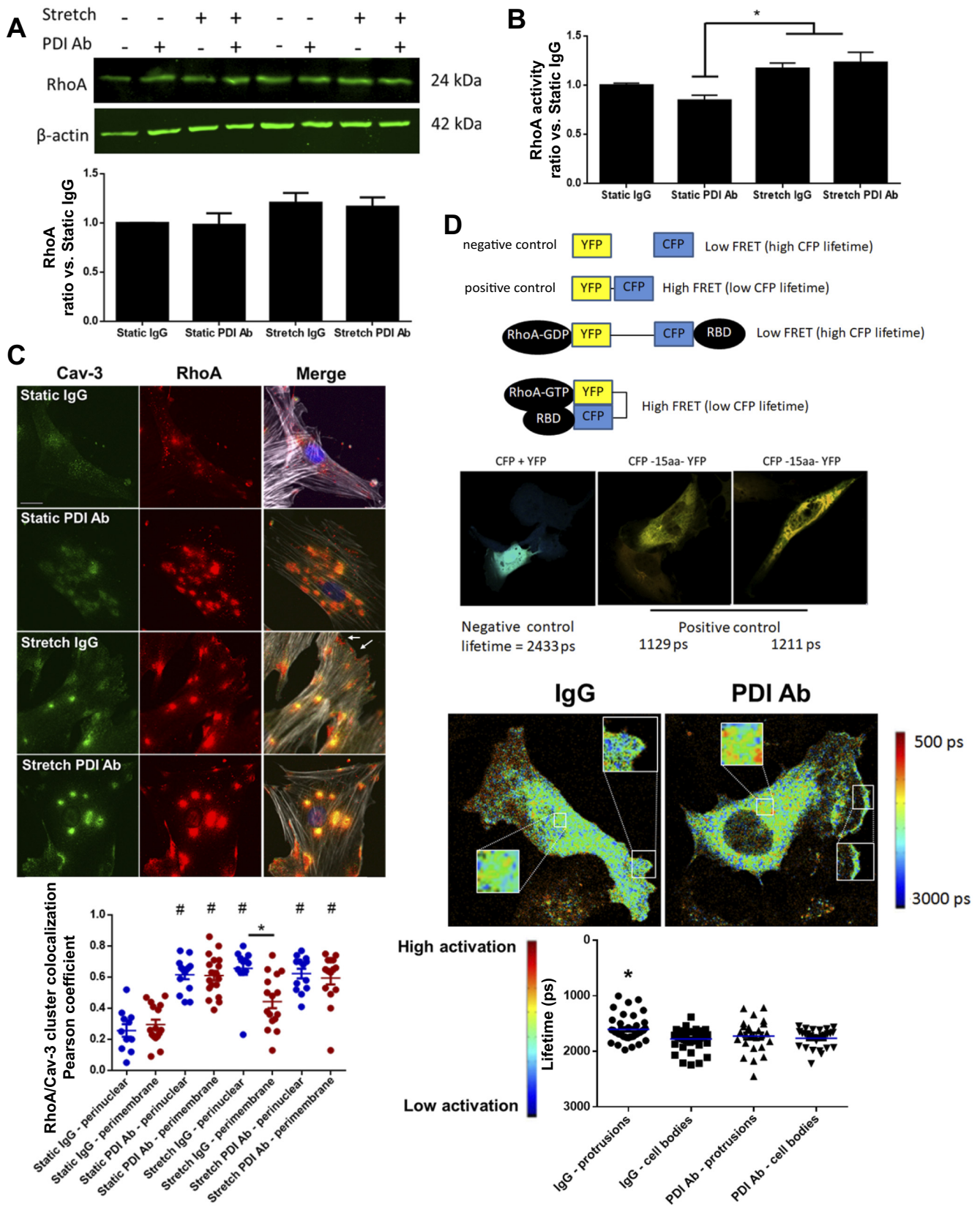
the spatial organization of RhoA activation. To further investigate this question, VSMCs were transfected with a RhoA activity FRET-based fluorescence biosensor (28). In this construct, RhoA attached to YFP, if active, i.e., GTP bound, promotes FRET (and consequently decreased donor fluorescence lifetime) via the interaction with CFP attached to a Rho-binding domain, whereas if RhoA is inactive, the two fluorescence reporters are far apart and FRET does not occur (see schema in Fig. 6D as well as negative and positive FRET controls). Our results (Fig. 6D) showed that cell protrusions presented higher RhoA activation than perinuclear regions (see METHODS), and this effect was lost by pecPDIA1 neutralization. Thus, a downstream mechanism targeted by pecPDIA1 during the coordinated response to mechanostimulation involves the differential distribution of RhoA activation at the cell periphery.

Finally, it is known that local force stimulation promotes a global cellular response. The mechanisms responsible for this effect include the release of mechanoresponsive factors such as thrombospondin and VEGF, which reportedly mediate stretch-induced effects on endothelial cell-to-VSMC and VSMC-to-VSMC communication, respectively (25, 33). To investigate whether pecPDIA1 could affect such paracrine regulatory loops, we performed a short-term incubation of static cells with the conditioned medium of VSMCs submitted or not to cyclic stretch (Fig. 7A). Inhibition of pecPDIA1 under basal conditions accentuated fiber thickening (Fig. 7B). However, the observed stress fiber buildup by conditioned medium from stretched VSMCs was markedly disrupted by pecPDIA1 inhibition (Fig. 7B). We next tested the effects of forced RhoA activation (CN01 incubation for 30 min). At static baseline, but not after PDI antibody incubation, CN01 plus conditioned medium exposure enhanced stress fiber thickness versus conditioned medium exposure alone (Fig. 7B). Moreover, CN01 was able to restore stress fiber buildup after stretch (Fig. 7C), reinforcing the notion that actin-cytoskeleton modulation by pecPDIA1 involves RhoA regulation.

DISCUSSION

We report that pecPDIA1 is a mechanism exerting a central upstream organizing role in actin cytoskeleton remodeling during cellular adaptation to a series of mechanobiological stimuli, which comprise models exploring diverse aspects of cellular responses. The pathways involved in pecPDIA1-associated cytoskeletal effects likely involve redox and nonredox processes integrated at several levels of systematic hierarchy.

An important question is what, if anything, makes PDIA1 distinctive among other thiol oxidoreductases. PDIA1 reacts only slowly with hydrogen peroxide, contrarily to peroxiredoxins, and thus is unlikely, as the latter, to behave as a mass peroxide sensor (26, 34). Meanwhile, the redox potential of PDIA1 is more oxidizing than that of thioredoxin, so that oxidized PDIA1 can more robustly sustain its disulfide form under a wider range of reducing potentials (34). Also, oxidized PDIA1 changes its conformation to an open state and enhances its chaperone activity (37), potentially exerting conformational changes in single or multiple targets. These effects are relevant, as we showed that PDIA1 is redistributed to more oxidizing cellular compartments during cyclic VSMC stretch (Fig. 3A). Thus, pecPDIA1 redox effects, just like those of intracellular PDI, are likely focal and target-oriented, rather than general large-scale changes in redox homeostasis.

Integrins are among the best-characterized pecPDIA1 targets (15). It is known that pecPDIA1, as well as Erp57 (PDIA3) and Erp5 (PDIA6), all reported in platelets, endothelial cells, and the vessel wall, can exert thiol reductase effects supportive of integrin transition from the extended moderate affinity to the extended high-affinity conformation, enhancing thrombosis formation (15), among several other effects. Indeed, we (35) previously reported that pecPDIA1 sustains β_1-integrin expression and thiol reduction during arterial repair postinjury. However, during the VSMC stretch response, pecPDIA1 supports a prooxidase effect on β_1-integrin (Fig. 2F). This is similar to the effect observed on α_5-integrin in endothelial cells submitted to acute laminar shear stress. Possibly, distinct stages of the time course of cytoskeleton remodeling cycles may explain these differences. Such thiol oxidase effect of pecPDIA1 is consistent with the observed PDIA1 redistribution to oxidant (sulfenate)-rich compartments during stretch. In fact, local increases in sulfenate adducts reportedly support cell migration (5). Also, this effect is in line with our previous results indicating that newly synthetized PDIA1 supports PDGF-induced superoxide production from Nox1 to sustain cell migration (29). Further studies are necessary to understand which are the oxidant sources sustaining the pecPDIA1 prooxidizing effect. Given our previous results (13), Nox NADPH oxidases are possible candidates; however, recent studies have shown conflicting data concerning the Nox subtype (Nox4 vs. Nox1) involved in cell orientation to stretch (23, 30).

Given the robust pecPDIA1-mediated integrin regulation, one can ask whether overall cytoskeletal PDI effects can be solely a consequence of that event. Our data with VSMC

Fig. 6. Peri/epicellular pool of protein disulfide isomerase-A1 (pecPDIA1) supports localized RhoA signaling. Primary rabbit aortic vascular smooth muscle cells (VSMCs) kept under static conditions or submitted to 24-h stretch (as in Fig. 1A) were incubated with PDI antibody (PDI Ab) or IgG. A: graph showing results of Western blot analysis of total RhoA expression. $n = 3$. B: total RhoA-GTPase activity measurement using G-LISA kit by fast-processing samples. *$P < 0.05$ for static PDI Ab vs. stretch groups. C: immunofluorescence analysis of caveolin-3 (left, Alexa 488 nm, green) and RhoA (middle, Alexa 546 nm, red) in nonpermeabilized static and stretched VSMCs prepared as in A. D: schema showing fluorescence resonance energy transfer (FRET) measurements for local RhoA activation by Fluorescence Lifetime (FLIM) detection system. Top: negative cyan fluorescent protein (CFP) + yellow fluorescent protein (YFP) and positive controls (CFP-15 aa-YFP) were assayed using plasmid constructions of separated CFP and YFP or connected by 15 amino acids, respectively. Middle: representative images of negative and positive controls showing the CFP lifetime. Bottom: local RhoA activity was measured using the RhoA-FLARE biosensor. First, primary rabbit VSMCs were transfected with a plasmid codifying RhoA connected to a flexible domain followed by a portion of the Rho-binding domain (RBD). Fluorescent proteins YFP and CFP were inserted at the NH_2 and COOH termini of the plasmid. When RhoA is in its GTP form, the RBD binds to RhoA, bringing the fluorophores to close proximity and inducing FRET, which was calculated using FLIM approach, as shown at the top schema. Donor (CFP) fluorescent lifetime is inversely proportional to RhoA activation and is depicted by color scale map (lifetime in picoseconds). Graph showing lifetime measurements at cell regions close to the nucleus (cell bodies) and at cell protrusions is presented on the bottom. Values ranged between negative and positive FRET/FLIM controls (see METHODS). *$P < 0.05$ for IgG protrusions vs. IgG cell bodies and PDI Ab cell bodies.
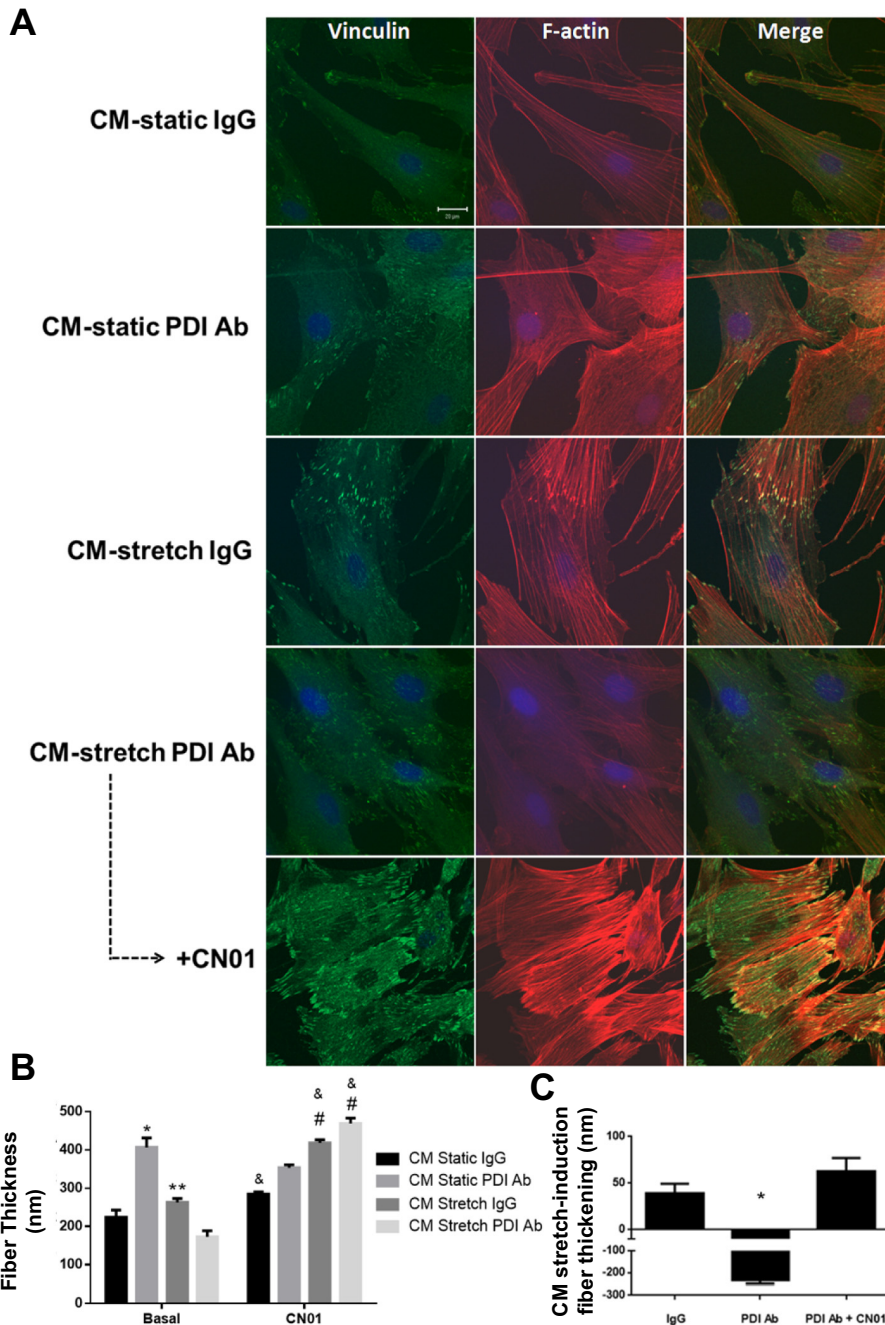
Fig. 7. Peri/epicellular pool of protein disulfide isomerase-A1 (pecPDIA1) regulates static and stretch-induced paracrine effect on cytoskeleton assembly. *A*: conditioned medium (CM) from cells submitted to static or stretch (CM-static and CM-stretch) conditions and exposed to either PDI antibody (PDI Ab) or IgG as in Fig. 1*A* were collected, centrifuged (2,000 rpm/10 min, 4°C), and incubated with static vascular smooth muscle cells (VSMCs). Alternatively, CMs were treated with the Rho activator CN01 (0.5 U/ml) during the last 30 min (+CN01). Staining for F-actin (*middle*, Alexa-phalloidin 635 nm, red) and vinculin (*left*, Alexa 488 nm, green) are shown. Nuclei were labeled with DAPI (blue) and merged images are shown on the *right*. $n = 3$. Scale bar = 20 μm. *B*: graph showing mean fiber thickness. *$P < 0.05$ vs. basal groups; **$P < 0.05$ vs. basal stretch PDI Ab; #$P < 0.05$ vs. CN01 static; &$P < 0.05$ vs. its respective basal. *C*: graph showing fiber thickening induction by CM from stretched cells (static IgG vs. stretch IgG and static PDI Ab vs. stretch PDI Ab or stretch PDI Ab + CN01). *$P < 0.05$ vs. CM-stretch induced IgG and PDI Ab + CN01. $n = 15$–18 cells from 3 independent experiments.

migration clearly indicate this is not the case, as pecPDIA1 neutralization impairs migration directionality/persistence, whereas total PDIA1 silencing with siRNA markedly disables all variables related to cell motility (Fig. 4*A* and Ref. 29). Besides integrins, myosin motors or focal adhesion regulation might also be involved in pecPDIA1 effects. We did not observe an effect of pecPDIA1 neutralization on myosin kinase-2 or neural Wiskott-Aldrich syndrome protein (n*WASP*) phosphorylation (data not shown), known to associate with force production (38). However, pecPDIA1 neutralization disturbed the overall pattern of Tyr[397] FAK phosphorylation, indicating impaired focal adhesion assembly. Overall, perturbation of force generation resulted in enhanced noise in force

distribution at baseline and during PDGF-induced migration, as shown by traction force microscopy (Fig. 5*A*). Similarly, pecPDIA1 neutralization at the VSMC surface impairs its mechanoresponse to paracrine-dependent mechanosignals (Fig. 7). Of note, our results indicate that secreted PDIA1 itself does not seem to behave as such a paracrine mechanosignal, since removal of pecPDIA1 from stretch-conditioned medium did not prevent focal adhesion and actually accentuated stress fiber induction (data not shown).

Our data indicated the convergence of PDIA1 with the integrin-RhoA-FAK axis regarding focal organization of Rho-GTPase activation to polarize VSMC responses. This is in line with prior evidence from our group showing that PDIA1

supports Rho-GTPase activation (29). Moreover, we recently reported that genes coding for PDIA1 and other PDI family members exhibit an intriguing and extremely conserved microsyntenic arrangement with genes coding for Rho guanine dissociation inhibitors (24), well-known Rho-GTPase regulators (11). In addition, PDIA1 interacts with Rho-GDIα, suggesting that the functional interactions may have supported the maintenance of this cluster arrangement (24). Rho-GTPases are widely involved with mechanoadaptation regulation. RhoA is known to translate external forces and migratory stimuli into cytoskeleton dynamics coordination. Local RhoA activation promotes cell orientation during uniaxial stretch (16). However, mechanisms governing localized RhoA activation during mechanoadaptation are unclear. One possibility is the targeting of Rho-GTPases, including RhoA, to specific membrane microdomains such as caveolae (19). Our results indicate that RhoA is targeted to scattered domains containing caveolin-3 clusters, but, under stretch, a membrane surface RhoA pool away from caveolin-3 is evident. This pattern, however, is disrupted upon pecPDIA1 inhibition, indicating that redistribution of active membrane-bound RhoA away from caveolae during mechanostimuli may support pecPDIA1-mediated regulation of cytoskeletal organization. We believe that this effect directly relates to integrin regulation, but other interactions may also be responsible, an issue deserving further investigation. Our results with the RhoA activity sensor further support that localized RhoA activation underlie pecPDIA1-induced noise reduction in cytoskeletal reorganization.

An increasing number of effects have been associated with pecPDIA1, including thrombosis, nitric oxide internalization, migration, regulation of disintegrin and metalloproteinase domain-containing protein 17, activation of transforming growth factor-β, internalization of phosphatidylserine, virus internalization, and others (34). Since redox modulation of specific cell surface targets related to cytoskeletal reorganization and cell adhesion is likely to modulate each of these effects, our results may help clarify multiple processes (36). Understanding how pecPDIA1 synergizes and interacts with intracellular PDIA1 is likely to shed light onto important integrative pathways governing adaptation to mechanical forces, involving mechanosensing, transmission, and effector responses (36). The reported effects of pecPDIA1 in vascular remodeling (35) are directly related to this paradigm. The results presented here implicate pecPDIA1 as a novel regulator of tensional homeostasis (36), able to connect redox processes (e.g., protein sulfenylation) mediated by mechanostimulation (stretch) in local mechanosensor activation (integrins) to recruit mechanotransmitter (RhoA) that drives mechanocomponents (actin-related proteins) into a final coordinated mechanoresponse (cell repositioning and directional migration), resulting in noise-suppressed cytoskeletal reorganization. Overall, the present work provides a novel additional mechanistic piece to support such a mechanobiological/redox model of vascular remodeling (36).

AUTHOR CONTRIBUTIONS

L.Y.T. and F.R.L. conception and design of research; L.Y.T., T.L.A., A.I.R., M.S.F., V.B.P., and A.M.d.S. performed experiments; L.Y.T., T.L.A., A.I.R., M.S.F., V.B.P., M.C.C.M., A.M.d.S., C.L.C., A.F.R., A.M.A., and F.R.L. analyzed data; L.Y.T., M.C.C.M., C.L.C., A.F.R., A.M.A., and F.R.L. interpreted results of experiments; L.Y.T., M.C.C.M., and A.F.R. prepared figures; L.Y.T. and F.R.L. drafted manuscript; L.Y.T., M.C.C.M., A.F.R., and F.R.L. edited and revised manuscript; L.Y.T., T.L.A., A.I.R., M.S.F., V.B.P., M.C.C.M., A.M.d.S., C.L.C., A.F.R., A.M.A., and F.R.L. approved final version of manuscript.

REFERENCES

1. **Araujo TLS, Zeidler JD, Oliveira PVS, Dias MH, Armelin HA, Laurindo FRM.** Protein disulfide isomerase externalization in endothelial cells follows classical and unconventional routes. *Free Radic Biol Med* 103: 199–208, 2017. doi:10.1016/j.freeradbiomed.2016.12.021.

2. **Benham AM.** The protein disulfide isomerase family: key players in health and disease. *Antioxid Redox Signal* 16: 781–789, 2012. doi:10.1089/ars.2011.4439.

3. **Burgess A, Vigneron S, Brioudes E, Labbé JC, Lorca T, Castro A.** Loss of human Greatwall results in G2 arrest and multiple mitotic defects due to deregulation of the cyclin B-Cdc2/PP2A balance. *Proc Natl Acad Sci USA* 107: 12564–12569, 2010. doi:10.1073/pnas.0914191107.

4. **Butler JP, Tolić-Nørrelykke IM, Fabry B, Fredberg JJ.** Traction fields, moments, and strain energy that cells exert on their surroundings. *Am J Physiol Cell Physiol* 282: C595–C605, 2002. doi:10.1152/ajpcell.00270.2001.

5. **Cameron JM, Gabrielsen M, Chim YH, Munro J, McGhee EJ, Sumpton D, Eaton P, Anderson KI, Yin H, Olson MF.** Polarized cell motility induces hydrogen peroxide to inhibit cofilin via cysteine oxidation. *Curr Biol* 25: 1520–1525, 2015. doi:10.1016/j.cub.2015.04.020.

6. **Crescente M, Pluthero FG, Li L, Lo RW, Walsh TG, Schenk MP, Holbrook LM, Louriero S, Ali MS, Vaiyapuri S, Falet H, Jones IM, Poole AW, Kahr WH, Gibbins JM.** Intracellular trafficking, localization, and mobilization of platelet-borne thiol isomerases. *Arterioscler Thromb Vasc Biol* 36: 1164–1173, 2016. doi:10.1161/ATVBAHA.116.307461.

7. **Dajnowiec D, Langille BL.** Arterial adaptations to chronic changes in haemodynamic function: coupling vasomotor tone to structural remodelling. *Clin Sci (Lond)* 113: 15–23, 2007. doi:10.1042/CS20060337.

8. **Damughatla AR, Raterman B, Sharkey-Toppen T, Jin N, Simonetti OP, White RD, Kolipaka A.** Quantification of aortic stiffness using MR elastography and its comparison to MRI-based pulse wave velocity. *J Magn Reson Imaging* 41: 44–51, 2015. doi:10.1002/jmri.24506.

9. **Datla SR, McGrail DJ, Vukelic S, Huff LP, Lyle AN, Pounkova L, Lee M, Seidel-Rogol B, Khalil MK, Hilenski LL, Terada LS, Dawson MR, Lassègue B, Griendling KK.** Poldip2 controls vascular smooth muscle cell migration by regulating focal adhesion turnover and force polarization. *Am J Physiol Heart Circ Physiol* 307: H945–H957, 2014. doi:10.1152/ajpheart.00918.2013.

10. **Dobrin PB.** Mechanical properties of arteries. *Physiol Rev* 58: 397–460, 1978. doi:10.1152/physrev.1978.58.2.397.

11. **Dovas A, Couchman JR.** RhoGDI: multiple functions in the regulation of Rho family GTPase activities. *Biochem J* 390: 1–9, 2005. doi:10.1042/BJ20050104.

12. **Eble JA, de Rezende FF.** Redox-relevant aspects of the extracellular matrix and its cellular contacts via integrins. *Antioxid Redox Signal* 20: 1977–1993, 2014. doi:10.1089/ars.2013.5294.

13. **Fernandes DC, Manoel AH, Wosniak J Jr, Laurindo FR.** Protein disulfide isomerase overexpression in vascular smooth muscle cells induces spontaneous preemptive NADPH oxidase activation and Nox1 mRNA expression: effects of nitrosothiol exposure. *Arch Biochem Biophys* 484: 197–204, 2009. doi:10.1016/j.abb.2009.01.022.

14. **Fernandes DC, Wosniak J Jr, Pescatore LA, Bertoline MA, Liberman M, Laurindo FR, Santos CX.** Analysis of DHE-derived oxidation prod-

ucts by HPLC in the assessment of superoxide production and NADPH oxidase activity in vascular systems. *Am J Physiol Cell Physiol* 292: C413–C422, 2007. doi:10.1152/ajpcell.00188.2006.

15. **Flaumenhaft R, Furie B.** Vascular thiol isomerases. *Blood* 128: 893–901, 2016. doi:10.1182/blood-2016-04-636456.

16. **Goldyn AM, Rioja BA, Spatz JP, Ballestrem C, Kemkemer R.** Force-induced cell polarisation is linked to RhoA-driven microtubule-independent focal-adhesion sliding. *J Cell Sci* 122: 3644–3651, 2009. doi:10.1242/jcs.054866.

17. **Hahn C, Schwartz MA.** Mechanotransduction in vascular physiology and atherogenesis. *Nat Rev Mol Cell Biol* 10: 53–62, 2009. doi:10.1038/nrm2596.

18. **Janiszewski M, Lopes LR, Carmo AO, Pedro MA, Brandes RP, Santos CX, Laurindo FR.** Regulation of NAD(P)H oxidase by associated protein disulfide isomerase in vascular smooth muscle cells. *J Biol Chem* 280: 40813–40819, 2005. doi:10.1074/jbc.M509255200.

19. **Kawamura S, Miyamoto S, Brown JH.** Initiation and transduction of stretch-induced RhoA and Rac1 activation through caveolae: cytoskeletal regulation of ERK translocation. *J Biol Chem* 278: 31111–31117, 2003. doi:10.1074/jbc.M300725200.

20. **Krishnan R, Klumpers DD, Park CY, Rajendran K, Trepat X, van Bezu J, van Hinsbergh VW, Carman CV, Brain JD, Fredberg JJ, Butler JP, van Nieuw Amerongen GP.** Substrate stiffening promotes endothelial monolayer disruption through enhanced physical forces. *Am J Physiol Cell Physiol* 300: C146–C154, 2011. doi:10.1152/ajpcell.00195.2010.

21. **Lahav J, Jurk K, Hess O, Barnes MJ, Farndale RW, Luboshitz J, Kehrel BE.** Sustained integrin ligation involves extracellular free sulfhydryls and enzymatically catalyzed disulfide exchange. *Blood* 100: 2472–2478, 2002. doi:10.1182/blood-2001-12-0339.

22. **Laurindo FR, Pescatore LA, de Castro Fernandes D.** Protein disulfide isomerase in redox cell signaling and homeostasis. *Free Radic Biol Med* 52: 1954–1969, 2012. doi:10.1016/j.freeradbiomed.2012.02.037.

23. **Montenegro MF, Valdivia A, Smolensky A, Verma K, Taylor WR, San Martín A.** Nox4-dependent activation of cofilin mediates VSMC reorientation in response to cyclic stretching. *Free Radic Biol Med* 85: 288–294, 2015. doi:10.1016/j.freeradbiomed.2015.05.011.

24. **Moretti AIS, Pavanelli JC, Nolasco P, Leisegang MS, Tanaka LY, Fernandes CG, Wosniak J Jr, Kajihara D, Dias MH, Fernandes DC, Jo H, Tran NV, Ebersberger I, Brandes RP, Bonatto D, Laurindo FRM.** Conserved gene microsynteny unveils functional interaction between protein disulfide isomerase and Rho guanine-dissociation inhibitor families. *Sci Rep* 7: 17262, 2017. doi:10.1038/s41598-017-16947-5.

25. **Ochoa CD, Baker H, Hasak S, Matyal R, Salam A, Hales CA, Hancock W, Quinn DA.** Cyclic stretch affects pulmonary endothelial cell control of pulmonary smooth muscle cell growth. *Am J Respir Cell Mol Biol* 39: 105–112, 2008. doi:10.1165/rcmb.2007-0283OC.

26. **Peixoto AS, Geyer RR, Iqbal A, Truzzi DR, Soares Moretti AI, Laurindo FRM, Augusto O.** Peroxynitrite preferentially oxidizes the dithiol redox motifs of protein disulfide isomerase. *J Biol Chem J Biol Chem* 293: 1450–1465, 2018. doi:10.1074/jbc.M117.807016.

27. **Pereira MB, Santos AM, Gonçalves DC, Cardoso AC, Consonni SR, Gozzo FC, Oliveira PS, Pereira AH, Figueiredo AR, Tiroli-Cepeda AO, Ramos CH, de Thomaz AA, Cesar CL, Franchini KG.** αB-crystallin interacts with and prevents stress-activated proteolysis of focal adhesion kinase by calpain in cardiomyocytes. *Nat Commun* 5: 5159, 2014. [Erratum in *Nat Commun* 6: 6508, 2015. 10.1038/ncomms7508. 25799360.] doi:10.1038/ncomms6159.

28. **Pertz O, Hodgson L, Klemke RL, Hahn KM.** Spatiotemporal dynamics of RhoA activity in migrating cells. *Nature* 440: 1069–1072, 2006. doi:10.1038/nature04665.

29. **Pescatore LA, Bonatto D, Forti FL, Sadok A, Kovacic H, Laurindo FR.** Protein disulfide isomerase is required for platelet-derived growth factor-induced vascular smooth muscle cell migration, Nox1 NADPH oxidase expression, and RhoGTPase activation. *J Biol Chem* 287: 29290–29300, 2012. doi:10.1074/jbc.M112.394551.

30. **Rodríguez AI, Csányi G, Ranayhossaini DJ, Feck DM, Blose KJ, Assatourian L, Vorp DA, Pagano PJ.** MEF2B-Nox1 signaling is critical for stretch-induced phenotypic modulation of vascular smooth muscle cells. *Arterioscler Thromb Vasc Biol* 35: 430–438, 2015. doi:10.1161/ATVBAHA.114.304936.

31. **Sadok A, Pierres A, Dahan L, Prévôt C, Lehmann M, Kovacic H.** NADPH oxidase 1 controls the persistence of directed cell migration by a Rho-dependent switch of alpha2/alpha3 integrins. *Mol Cell Biol* 29: 3915–3928, 2009. doi:10.1128/MCB.01199-08.

32. **Sathyanesan A, Ogura T, Lin W.** Automated measurement of nerve fiber density using line intensity scan analysis. *J Neurosci Methods* 206: 165–175, 2012. doi:10.1016/j.jneumeth.2012.02.019.

33. **Schad JF, Meltzer KR, Hicks MR, Beutler DS, Cao TV, Standley PR.** Cyclic strain upregulates VEGF and attenuates proliferation of vascular smooth muscle cells. *Vasc Cell* 3: 21, 2011. doi:10.1186/2045-824X-3-21.

34. **Soares Moretti AI, Martins Laurindo FR.** Protein disulfide isomerases: Redox connections in and out of the endoplasmic reticulum. *Arch Biochem Biophys* 617: 106–119, 2017. doi:10.1016/j.abb.2016.11.007.

35. **Tanaka LY, Araújo HA, Hironaka GK, Araujo TL, Takimura CK, Rodriguez AI, Casagrande AS, Gutierrez PS, Lemos-Neto PA, Laurindo FR.** Peri/epicellular protein disulfide isomerase sustains vascular lumen caliber through an anticonstrictive remodeling effect. *Hypertension* 67: 613–622, 2016. doi:10.1161/HYPERTENSIONAHA.115.06177.

36. **Tanaka LY, Laurindo FRM.** Vascular remodeling: a redox-modulated mechanism of vessel caliber regulation. *Free Radic Biol Med* 109: 11–21, 2017. doi:10.1016/j.freeradbiomed.2017.01.025.

37. **Wang C, Yu J, Huo L, Wang L, Feng W, Wang CC.** Human protein-disulfide isomerase is a redox-regulated chaperone activated by oxidation of domain a′. *J Biol Chem* 287: 1139–1149, 2012. doi:10.1074/jbc.M111.303149.

38. **Zhang W, Huang Y, Gunst SJ.** The small GTPase RhoA regulates the contraction of smooth muscle tissues by catalyzing the assembly of cytoskeletal signaling complexes at membrane adhesion sites. *J Biol Chem* 287: 33996–34008, 2012. doi:10.1074/jbc.M112.369603.